arXiv:1211.0570v1 [hep-ex] 2 Nov 2012

Improved Measurement of Electron Antineutrino Disappearance at Daya Bay

Xin Qian [1], on behalf of the Daya Bay Collaboration

Kellogg Radiation Laboratory, California Institute of Technology, Pasadena, CA

Abstract. The Daya Bay experiment was designed to be the largest and the deepest underground among the many current-generation reactor antineutrino experiments. With functionally identical detectors deployed at multiple baselines, the experiment aims to achieve the most precise measurement of $\sin^2 2\theta_{13}$. The antineutrino rates measured in the two near experimental halls are used to predict the rate at the far experimental hall (average distance of 1648 m from the reactors), assuming there is no neutrino oscillation. The ratio of the measured over the predicted far-hall antineutrino rate is then used to constrain the $\sin^2 2\theta_{13}$. The relative systematic uncertainty on this ratio is expected to be 0.2∼0.4%. In this talk, we present an improved measurement of the electron antineutrino disappearance at Daya Bay. With data of 139 days, the deficit of the antineutrino rate in the far experimental hall was measured to be 0.056 ± 0.007 (stat.) $\pm\, 0.003$ (sys.). In the standard three-neutrino framework, the $\sin^2 2\theta_{13}$ was determined to be 0.089 ± 0.011 at the 68% confidence level in a rate-only analysis.

Keywords: neutrino oscillation, neutrino mixing, reactor, Daya Bay
PACS: 14.60.Pq

INTRODUCTION

As fundamental particles in the standard model, (anti)neutrinos were initially thought to have zero mass. Such an assumption was supported by the experimental evidence that only left-handed neutrinos (also right-handed antineutrinos) were detected [1]. However, in the past decades, the phenomenon of neutrino flavor oscillation observed by Super-K, SNO, KamLAND, MINOS, and many other experiments successfully established the existence of non-zero neutrino masses and the neutrino mixing. A recent review can be found in Ref. [2]. The neutrino oscillations are commonly described by the Pontecorvo-Maki-Nakagawa-Sakata (PMNS) matrix and two neutrino mass-squared differences ($\Delta m^2_{32} := m^2_3 - m^2_2$ and $\Delta m^2_{21} := m^2_2 - m^2_1$) [3, 4, 5]. The PMNS matrix denotes the mixing between the neutrino flavor and mass eigenstates. It contains three mixing angles θ_{12}, θ_{23}, and θ_{13}, and an imaginary phase δ, referred to as the CP phase in the leptonic sector.

As of two year ago, θ_{13} was still the least known among all three neutrino mixing angles in the PMNS matrix. The best constraint was from CHOOZ reactor antineutrino experiment with $\sin^2 2\theta_{13} < 0.17$ at 90% confidence level (C.L.) [6, 7]. A global analysis [8] in 2008 including both solar and reactor neutrino data suggested a non-zero θ_{13}. However, in the past 18 months or so, an explosion of data from multiple experiments greatly enhanced our understanding of θ_{13}. In 2011, through measurements of ν_e appearance from a ν_μ beam, the long baseline experiments T2K [9] and MINOS [10] reported hints of a non-zero θ_{13} at about 2.5 and 1.4 standard deviations [2], respectively. In January 2012, the reactor antineutrino experiment Double-CHOOZ [11] also reported a hint of a non-zero θ_{13} at 1.6 standard deviations with a single detector. The Daya Bay experiment, with six functionally identical detectors at three locations, carried out a measurement of relative ratio of reactor antineutrino rates [12], which significantly improved the sensitivity to the $\sin^2 2\theta_{13}$. In March 2012, the Daya Bay collaboration announced a non-zero value of θ_{13} at 5.2 standard deviations [13]. About one month later, this finding was confirmed by the RENO reactor antineutrino experiment [14], which reported a consistent result using a ratio between antineutrino rates from two detectors. The Daya Bay experiment has since reported an improved measurement of the electron antineutrino disappearance [15] with 2.5 times of the previously reported statistics [13].

THE DAYA BAY EXPERIMENT

The Daya Bay experiment, located on the south coast of China (55 km northeast to Hong Kong and 45 km east to Shenzhen), was designed to provide the most precise measurement of θ_{13} with a sensitivity of $\sin^2 2\theta_{13} < 0.01$

---

[1] Email:xqian@caltech.edu

[2] Results from the long baseline experiments actually depend on the assumption of the neutrino mass hierarchy and value of CP phase δ.

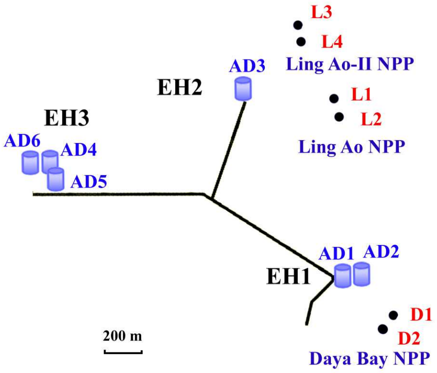

FIGURE 1. The layout of the Daya Bay experiment. The dots represent reactor cores, labeled as D1, D2, and L1-4. Six ADs were installed in three experimental halls during the reported analysis period.

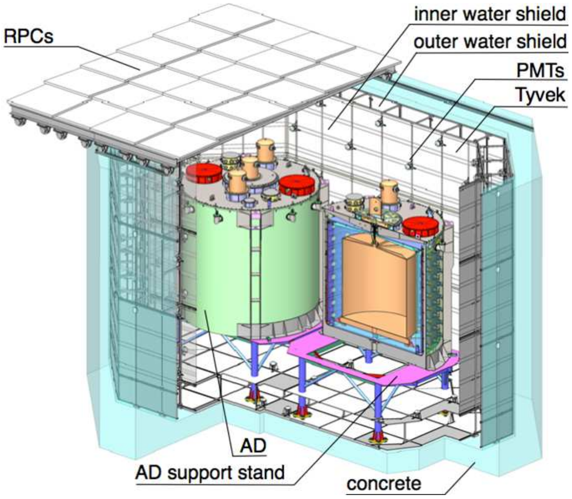

FIGURE 2. Layout of Daya Bay detectors in a near site.

at a 90% C.L. [16]. Such a measurement requires high accuracy and precision. The high accuracy is achieved by the combination of powerful reactors (17.6 GW thermal power) and large target mass (80 tons in the far hall). In addition, the location of the far detectors is optimized to obtain the best sensitivity to $\sin^2 2\theta_{13}$ with the current knowledge of Δm^2_{32}. To achieve high precision, the reactor-related systematic uncertainties are minimized by adapting the ratio method [12] with multiple detectors at multiple baselines. The detector-related systematic uncertainties are minimized by using identical detectors and performing precise detector calibrations. The background-related systematic uncertainties are minimized by placing detectors deep underground in order to reduce cosmic muon related backgrounds. Furthermore, passive shielding (water pools surrounding detectors) and active shielding (resistive-plate chambers above water pools) were implemented to tag the cosmic muons. The water pools also shield detectors from various environmental radioactive backgrounds.

Fig. 1 shows the layout of the Daya Bay experiment during this reported analysis period. There are six reactors grouped into three pairs. Each reactor contains a core with a maximum 2.9 GW thermal power. Three underground experimental halls (EHs) are connected with horizontal tunnels. The effective vertical overburdens are 250, 265, and 860 water-equivalent meters for EH1, EH2, and EH3, respectively. For this improved measurement, two, one, and three antineutrino detectors (ADs) were installed in EH1, EH2, and EH3, respectively. The distance from the six ADs to the six cores were surveyed with the Global Positioning System (GPS) above ground and Total Stations underground. The precision of distance was about 1.8 cm.

The antineutrinos in the Daya Bay experiment are detected through the inverse beta decay (IBD) process $\overline{\nu}_e + p \rightarrow e^+ + n$. The signature of such process is a prompt signal of the scintillation and subsequent annihilation of the position in the liquid scintillator (LS), followed shortly by a delayed signal with $\sim$8 MeV energy deposition when the neutron is captured by the Gadolinium (Gd) doped inside LS (0.1% in weight). The energy of neutrino can be deduced from the energy deposition of the prompt signal with $E_{\overline{\nu}} \approx E_{positron} + 0.8$ MeV. As shown in Fig. 2, the ADs adopt a three-zone cylindrical-shaped design, with the inner, middle, and outer zone containing 20 ton Gd-doped LS (Gd-LS), 20 ton LS, and 40 ton mineral oil, respectively. With load cells and an ISO tank, the target mass uncertainty of the 20 ton GD-LS is controlled to be only about 3 kg.

Each AD contains 192 8-inch photomultiplier tubes (PMTs) installed on the side walls. The photocathode coverage is about 8%, which is further enhanced to about 12% with a pair of optical reflectors at the top and bottom of each detector. The achieved detector energy resolution is parametrized as [17]

$$\frac{\delta E}{E} = \left(\frac{7.5}{\sqrt{E(\mathrm{MeV})}} + 0.9\right)\%, \qquad (1)$$

with respect to the visible energy E. The detector calibration is performed weekly with three automated calibration units (ACUs) per AD: two located above the center and the edge of the GD-LS region and one placed above the LS region. The ACUs are remotely controlled by a LabVIEW program and operated underwater. Each ACU contains four sources: a light-emitting diode (LED) for the PMT gain/timing calibration, a $\sim$15 Hz ^{68}Ge source for the threshold calibration of the IBD prompt signal, a $\sim$100 Hz ^{60}Co source for the high statistical determination of the overall energy scale, and a $\sim$0.5 Hz ^{241}Am-

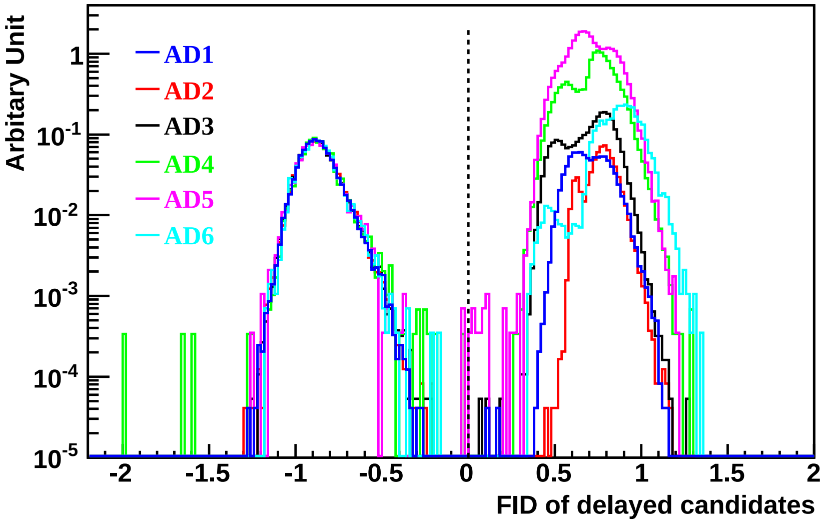

FIGURE 3. Discrimination of the flasher events (FID > 0) from the delayed signals of IBD (FID < 0). While the flasher events possess different distributions among different ADs, the delayed signals of IBD share the same distribution.

^{13}C neutron source to understand neutron captures on Gd and to determine the H/Gd ratio in the target region.

The muon detection system in each experimental hall consists of a high purity water pool surrounding the ADs and a layer of resistive plate chambers (RPC) above the water pool. The water pool is further divided into two optically separated regions, the inner water pool (IWS) and the outer water pool (OWS). Each region operates as an independent water Cerenkov detector, and can be used to cross calibrate each other. The muon detection efficiencies are measured to be 99.7% and 97% for the IWS and OWS [17], respectively. The water pool also plays a crucial role in shielding radioactive backgrounds. The distance between the edge of each AD to the closest wall is at least 2.5 m. The array of RPCs covering the entire water pool is used to provide additional tagging of cosmic muons.

SELECTION OF INVERSE BETA DECAY EVENTS

About 5% of the PMTs would spontaneously flash and emit light. Such events are called “flashers”. The reconstructed energy of such events covers a wide range, from sub-MeV to 100 MeV. A few features are observed when a PMT flashes: i) the charge fraction of the flashing PMT is high; ii) the surrounding PMTs as well as the ones located on the opposite side of the AD receive large fraction of light from the flashing PMT; and iii) the timing spread of all PMTs’ hits are generally wide. Accordingly, a few flasher identification (FID) variables were constructed to separate the good physics events from the flashing events. Fig. 3 shows the distribution of an FID variable deduced from the charge pattern for the IBD delay candidates. The good IBD events are well separated from the flasher events. Detailed description of the flasher discrimination can be found in Ref. [17]. The inefficiency of the IBD signals due to FID cuts is only about (0.024 ± 0.006)%, and the contamination of flashing events in the IBD sample is below 0.01%, which is further suppressed by the accidental background subtraction procedure.

After the flashing events are removed, the IBDs are further selected with the following cuts: i) the energy of the prompt signal is between 0.7 and 12 MeV; ii) the energy of the delay signal is between 6 and 12 MeV; and iii) the time difference between the prompt and the delay signal is between 1 and 200 μs. In addition, a multiplicity cut is applied to remove the energy ambiguities in the prompt signal. For example, one choice of the multiplicity cut requires no prompt-like signal 400 μs before the delay signal and no delay-like signal 200 μs after the delay signal [3]. The fixed time cut (relative to the delay signal) leads to simplified calculations of the efficiency and livetime of IBD events and the rate of accidental backgrounds. Correspondingly, three types of muon veto cuts are also applied to the delay signal in order to suppress backgrounds. The first one is for the water pool muon, which is defined as one IWS or OWS event with more than 12 PMT hits. The veto cut spans from 2 μs before to 600 μs after the water pool signal. The second one is for the AD shower muon, which is defined as one AD signal with more than 3×10^5 photoelectrons (PEs). The corresponding energy is about 1.8 GeV. The veto cut spans from 2 μs before to 0.4 s after the AD signal. The last one is for the AD non-shower muon, which is defined as one AD signal with its energy between 20 MeV and 1.8 GeV. The veto cut spans from 2 μs before to 1.4 ms after the AD signal. The choice of 2 μs before the muon signal in all three cuts is to leave enough room for the potential non-synchronization among different detectors. The AD shower muon veto is applied to suppress the long-lived ^{9}Li/^{8}He background. The AD non-shower muon veto is applied to suppress the fast neutron background. The overall detection efficiency for the IBD events is about 80%, with the Gd catpure ratio (84%) and the efficiency of the 6 MeV delay signal cut (91%) being the two leading contributors.

---

[3] The prompt-like and delay-like signals refer to events with energy 0.7-12 MeV and 6-12 MeV, respectively.

SUMMARY OF BACKGROUNDS

The largest contamination in the Daya Bay IBD sample is the accidental background with about 4.6% at the far site and about 1.7% at the near sites. An accidental background event arises when a delay-like signal and an unrelated prompt-like signal (usually radioactive events) accidentally fall within a 199 μs coincidence window. Such background ($R_{accidental}$) can be accurately calculated through Poisson statistics given the measured rates of single prompt-like events (R_p) and single delay-like events (R_d) [4]:

$$R_{accidental} = P(0,200\mu s\cdot R_p)\cdot P(1,199\mu s\cdot R_p) \cdot R_d\cdot P(0,200\mu s\cdot R_d). \quad (2)$$

Poisson function $P(n,\mu)=e^{-\mu}\frac{\mu^n}{n!}$ represents the probability of observing n events given an expectation value of μ events. The above calculation results in negligible systematic uncertainties. This method is cross-checked with an off-window coincidence method and a coincidence vertex method [15].

The second largest contamination at the far site is the correlated backgrounds from the Am-C neutron source. During the data taking, the Am-C neutron sources are parked inside the ACUs on top of the ADs. The energetic neutrons from these sources occasionally undergo an inelastic scattering with an iron nuclei resulting in gamma emissions, followed by a neutron capture on another iron nuclei with additional gamma emissions. When these gammas are emitted toward AD, it is possible these correlated events could mimic an IBD signal. The contamination from the Am-C source, which is about 0.3% (0.03%) at the far (near) site, is calculated through a GEANT4-based Monte Carlo simulation, which can reproduce the energy spectrum of single backgrounds from Am-C sources. The systematic uncertainty of this correlated background is assumed to be 100%.

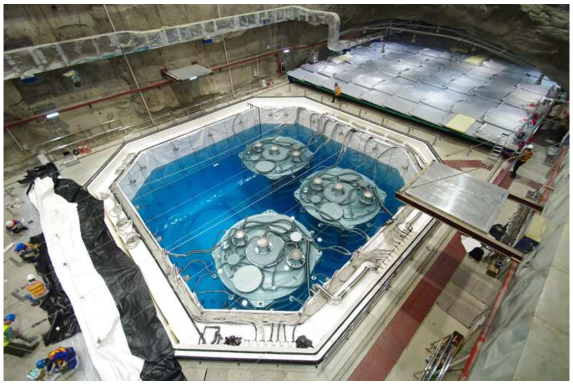

FIGURE 4. Three ADs were deployed in the EH3.

The ^{9}Li/^{8}He and the fast neutrons are two major IBD contamination caused by cosmic muons. The nucleus of ^{9}Li or ^{8}He are produced from the carbon nucleus when cosmic muons pass through the liquid scintillator. The ^{9}Li and ^{8}He, with half lifetime of 257 ms and 172 ms, respectively, are both long lifetime beta emitters. They would undergo a beta decay providing a prompt-like signal. The daughter nuclei could then undergo a spontaneous fission, with a neutron emission in the final state resulting in a delay-like signal. Such a pair of correlated prompt-like and delay-like signal would mimic an IBD event. The contamination of ^{9}Li/^{8}He can be directly measured by fitting the spectrum of time between the IBD candidate and the last tagged AD muon. The measured ^{9}Li/^{8}He rates from all three experimental halls are consistent with an empirical formula of $\alpha E_\mu^{0.74}$ given the average muon energy E_μ in each site. Furthermore, the contamination are suppressed by an optimized AD shower muon cut described in the previous section. The remaining contamination is about 0.2% (0.35%) for the far (near) site with a 50% systematic uncertainty due to the fitting procedure.

The fast neutron backgrounds are caused by the energetic neutrons produced inside or outside the muon veto system. These energetic neutrons can undergo an elastic scattering with protons, leaving a prompt-like signal due to the proton recoil, followed by the neutron thermalization and then neutron capture on Gd producing a delay-like signal. The energy of the proton recoil signals ranges from sub MeV to tens of MeV. Therefore, one can extrapolate the measured fast neutron's prompt en-

---

[4] The efficiency due to the fixed-time multiplicity cut is then $P(0,400\mu s\cdot R_p)\cdot P(0,200\mu s\cdot R_d)$.

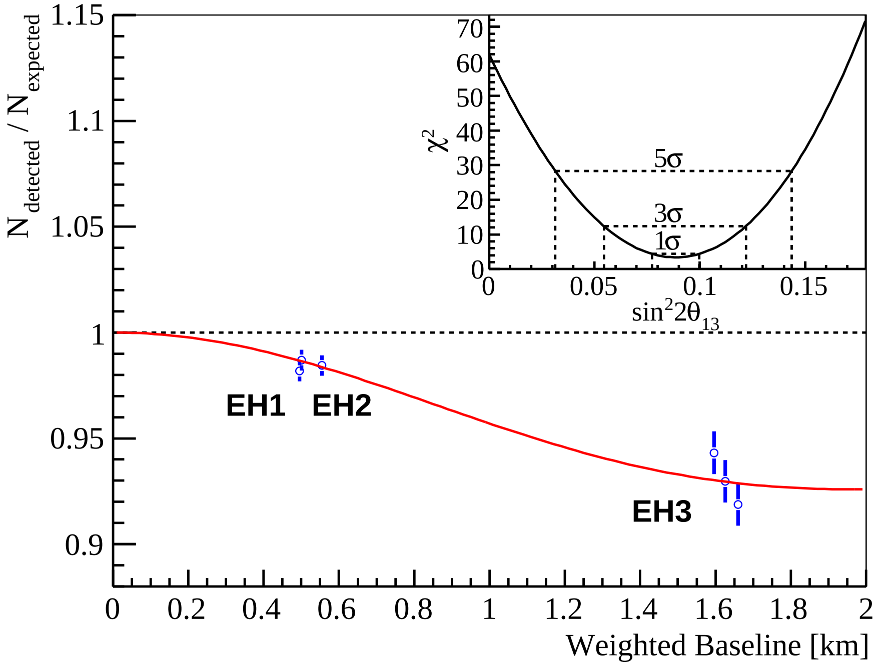

FIGURE 5. The ratio between the measured and the expected signals in each detector vs. the flux-weighted average baseline, which is computed with reactor and survey data. The expected signals have been corrected with the best fit normalization parameter assuming no oscillation. The error bars represent the uncorrelated uncertainties. The oscillation survival probability at the best-fit value is plotted as the smooth curve. For clarity purpose, the AD4/6 data points are shifted by -30 and 30 m, respectively. The χ^2 value vs. the $\sin^2 2\theta_{13}$ value is shown in the inner panel.

ergy spectrum above 15 MeV to the energy range of interests (0.7-12 MeV) in order to estimate the contamination in the IBD candidates. A flat background spectrum is assumed, which is confirmed by the spectrum of fast neutron events with muon tagging from water pools and RPC. The systematic uncertainty is constrained to about 30%. The contaminations due to fast neutron are estimated to be about 0.07% (0.12%) for the far (near) site.

The last contamination is the ^{13}C(α,n)^{16}O background caused by radioactivity inside ADs. The contamination is determined by Monte Carlo with measured alpha-decay rates. We identified four sources of alpha decays: the ^{210}Po events and the decay chains from ^{238}U, ^{232}Th, and ^{227}Ac. The backgrounds are calculated to be about 0.05% (0.01%) for the far (near) site with a 50% systematic uncertainty. Altogether, the total backgrounds in the IBD sample are thus determined to be $5 \pm 0.4\%$ and $2 \pm 0.2\%$ for the far site and near sites, respectively.

OSCILLATION ANALYSIS

The oscillation analysis includes data of 139 days (Dec. 24th 2011 - May 11th, 2012) with six ADs. Fig. 4 shows a picture of the three ADs in the EH3. The analysis pro-

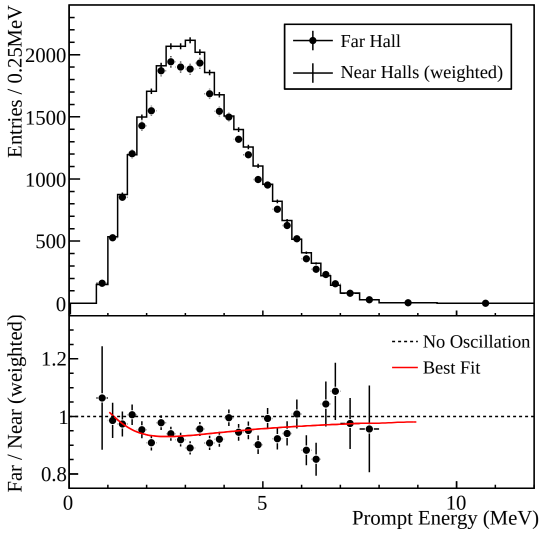

FIGURE 6. Top panel: Measured prompt energy spectrum at the far site (sum of three ADs) is compared with the predicted spectrum based on the measurements at the two near sites assuming no oscillation. Backgrounds are subtracted. Only statistical uncertainties are shown. Bottom panel: The ratio of the measured over the expected (no-oscillation) spectrum. The solid curve is the expected ratio vs. the true prompt energy with the neutrino oscillation for $\sin^2 2\theta_{13} = 0.089$.

cedure is described in details in Ref. [13, 15]. Since different experimental halls have different mountain overburdens, they also observe different muon rates. The average muon veto efficiency for six ADs in the three experimental halls are 0.8231, 0.8198 (EH1), 0.8576 (EH2), and 0.9813, 0.9813, 0.9810 (EH3). Besides the background-related uncertainties, the largest uncorrelated detector-related uncertainty (0.12%) is due to the 6 MeV energy cut in selecting delay signals. Other sizable uncorrelated detector-related uncertainties include 0.1% from the neutron Gd capture ratio, 0.03% from the number of target protons, and 0.02% from the spill-in effect. (The spill-in effect refers to that the IBD neutrons generated outside but captured inside the target GD-LS region outnumber the IBD neutrons generated inside but captured outside the GD-LS region. The reason for such imbalance is that thermal neutrons have a larger cross section to be captured on the Gd than the proton.) With the ratio method, the correlated detector-related uncertainty (about 1.9% in total) has negligible effects on the oscillation analysis. The same applies to the correlated reactor-related uncertainty. The uncorrelated reactor-related uncertainties include 0.5% from the received thermal power data, 0.6% from the calculated fission fractions, and 0.3% from the antineutrinos produced by the spent fuel. The total uncorrelated reactor-related uncertainty is 0.8%, which is further suppressed by about a factor of 20 in the oscillation analysis due to the multiple core/reactors configuration at Daya Bay.

The final antineutrino rates per day in the six ADs of three experimental halls, after corrections of the livetime, the veto efficiencies, and the background, are 662.47±3.00, 670.87±3.01 (EH1), 613.53±2.69 (EH2), and 77.57±0.85, 76.62±0.85, 74.97±0.84 (EH3). In the same experimental hall, the differences of AD rates stemming from ADs' different locations are consistent with expectation within statistical uncertainties. The deficit of antineutrino rate at the far site is quantified by the ratio of the measured far-hall IBD rate over the expected rate, which is calculated with the measured IBD rates of the near detectors assuming no oscillation. The resulting deficit is 0.056 ± 0.007 (stat.) ± 0.003 (sys.).

The chi-square method with pull terms is used to extract $\sin^2 2\theta_{13}$ within the standard 3-flavor oscillation model, in which the disappearance probability of the electron antineutrino is written as:

$$\begin{aligned} P(\bar{\nu_e} \to \bar{\nu_e}) &= 1 - \sin^2 2\theta_{13} \cos^2 \theta_{12} \sin^2 \Delta_{31} \\ &\quad - \sin^2 2\theta_{13} \sin^2 \theta_{12} \sin^2 \Delta_{32} \\ &\quad - \cos^4 \theta_{13} \sin^2 2\theta_{12} \sin^2 \Delta_{21}, \qquad (3) \end{aligned}$$

with $\Delta_{ij} \equiv |\Delta_{ij}| = 1.27|\Delta m^2_{ij}| \frac{L(m)}{E(MeV)}$. In this framework, the uncertainties from the backgrounds, detectors, reactor fluxes, and the oscillation parameters are taken into account properly in a consistent manner. The $\sin^2 2\theta_{13}$ is determined to be 0.089±0.011. Fig. 5 shows the ratios of measured over expected IBD rates vs. weighted baseline for all ADs. The data are compared with the expected oscillation curve (red-solid line). Our improved measurement disfavors the $\sin^2 2\theta_{13} = 0$ hypothesis at a 7.7 standard deviations.

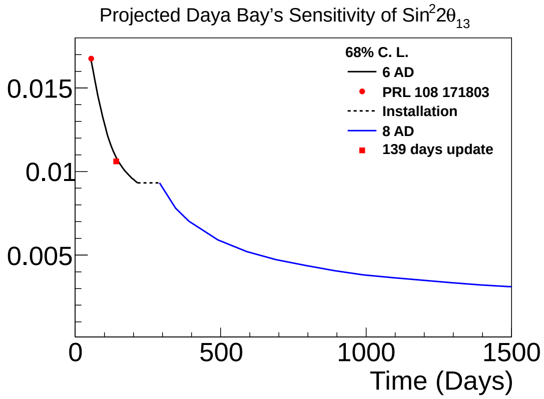

FIGURE 7. Projected $\sin^2 2\theta_{13}$'s sensitivity in terms of half of the 68% confidence interval of Daya Bay vs. the running time. The published and improved Daya Bay results are shown as red dots. The period of 6-AD data taking (black) is separated from the period of 8-AD data taking (blue) by an installation/calibration period (dashed).

CONCLUSION AND OUTLOOK

In this talk, we reported an improved measurement of electron antineutrino disappearance at Daya Bay. The new results with 2.5 times more data confirms the previously published results [13], and improves the precision of $\sin^2 2\theta_{13}$. Currently, the total uncertainty is still dominated by the statistical uncertainty, which is about a factor of 2 larger than the systematic uncertainty. Fig. 7 shows the projected sensitivity of $\sin^2 2\theta_{13}$ in terms of half of the 68% confidence interval with respect to the running time. With the full 8-AD configuration, we expect to achieve a $\sim 5\%$ measurement of $\sin^2 2\theta_{13}$ in about 3 years. Furthermore, the Daya Bay experiment also has the potential to measure the effective squared-mass difference Δm^2_{ee}, which is a combination of Δm^2_{31} and Δm^2_{32}, through the measurement of IBD energy spectrum distortion. Due to the short baseline < 2 km, the measurement of Δm^2_{ee} is not sensitive to the neutrino mass hierarchy (sign of Δm^2_{32}) [18]. In addition, the high statistics IBD samples from Daya Bay would provide the most precise measurement of the antineutrino energy spectrum, which is essential for the future measurements with reactor antineutrinos.

With the global efforts led by the Daya Bay experiment, the $\sin^2 2\theta_{13}$ is found to be around 0.09. Such a large value of $\sin^2 2\theta_{13}$ opens doors to two of the remaining unknown parameters in the neutrino sector, the CP phase δ in the leptonic sector and the neutrino Mass Hierarchy [5]. In particular, the long baseline experiments [20, 21, 22, 23] can provide essential information for both parameters through the (anti)ν_e appearance from a (anti)ν_μ beam. Meanwhile, the possibility of utilizing a medium baseline (∼60 km) reactor neutrino experiment to determine the neutrino mass hierarchy is also intensively discussed [24, 25, 26, 27, 18, 28]. We therefore expect a new era of discovery in the next couple of decades.

ACKNOWLEDGMENTS

We would like to thank the support from Caltech and the National Science Foundation. The Daya Bay experiment is supported in part by the Ministry of Science and Technology of China, the United States Department of Energy, the Chinese Academy of Sciences, the National Natural Science Foundation of China, the Guangdong provincial government, the Shenzhen municipal government, the China Guangdong Nuclear Power Group, Shanghai Laboratory for Particle Physics and Cosmology, the Research Grants Council of the Hong Kong Special Administrative Region of China, University Development Fund of The University of Hong Kong, the MOE program for Research of Excellence at National Taiwan University, National Chiao-Tung University, and NSC fund support from Taiwan, the U.S. National Science Foundation, the Alfred P. Sloan Foundation, the Ministry of Education, Youth and Sports of the Czech Republic, the Czech Science Foundation, and the Joint Institute of Nuclear Research in Dubna, Russia. We thank Yellow River Engineering Consulting Co., Ltd. and China railway 15th Bureau Group Co., Ltd. for building the underground laboratory. We are grateful for the ongoing cooperation from the China Guangdong Nuclear Power Group and China Light & Power Company.

REFERENCES

1. M. Goldhaber, L. Grodzins, and A. W. Sunyar, Phys. Rev. **109**, 1015 (1958).
2. R. D. McKeown and P. Vogel, Phys. Rep. **394**, 315 (2004).
3. B. Pontecorvo, Sov. Phys. JETP **6**, 429 (1957).
4. B. Pontecorvo, Sov. Phys. JETP **26**, 984 (1968).
5. Z. Maki, M. Nakagawa, and S. Sakata, Prog. Theor. Phys. **28**, 870 (1962).
6. M. Apollonio *et al.* [CHOOZ Collaboration], Phys. Lett. **B466**, 415 (1999).
7. M. Apollonio *et al.* [CHOOZ Collaboration], Eur. Phys. J. **C27**, 331 (2003).
8. G. Fogli *et al.*, Phys. Rev. Lett. **101**, 141801 (2008).
9. K. Abe *et al.* [T2K Collaboration], Phys. Rev. Lett. **107**, 041801 (2011).
10. P. Adamson *et al.* [MINOS Collaboration], Phys. Rev. Lett. **107**, 181802 (2011).
11. Y. Abe *et al.* [Double Chooz Collaboration], Phys. Rev. Lett. **108**, 131801 (2012).
12. L. A. Mikaelyan and V. V. Sinev, Phys. Atom. Nucl. **63**, 1002 (2000).
13. F. P. An *et al.* [Daya Bay Collaboration], Phys. Rev. Lett. **108**, 171803 (2012).
14. J. K. Ahn *et al.* [RENO Collaboration], Phys. Rev. Lett. **108**, 191802 (2012).
15. F. P. An *et al.*[Daya Bay Collaboration], arXiv:1210.6327 (2012), submitted to Chinese Physics C.
16. Daya Bay Collaboration, arXiv:hep-ex/0701029 (2006).
17. F. P. An *et al.* [Daya Bay Collaboration], Nucl. Inst. Method **A685**, 78 (2012).
18. X. Qian *et al.*, arXiv:1208.1551 (2012), submitted to Phys. Rev. D.
19. X. Qian *et al.*, arXiv:1210.3651 (2012), submitted to Phys. Rev. D.
20. K. Abe *et al.* [T2K Collaboration] arXiv:1106.1238 (2011).
21. D. Ayres *et al.* [NOνA Collaboration] The NOνA Technical Design Report. FERMILAB-DESIGN-2007-01 (2007).
22. T. Akiri *et al.* [LBNE Collaboration], arXiv:1110.6249 (2011).
23. K. Abe *et al.* [Hyper-K Collaboration], arXiv:1109.3262 (2011).
24. S. Choubey, S. T. Petcov, and M. Piai, Phys. Rev. **D68**, 113006 (2003).
25. J. G. Learned *et al.* Phys. Rev. **D78**, 071302R (2008).
26. L. Zhan *et al.* Phys. Rev. **D78**, 111103R (2008).
27. L. Zhan *et al.* Phys. Rev. **D79**, 073007 (2009).
28. E. Ciuffoli, J. Evaslin, and X. M. Zhang, arXiv:1209.2227 (2012).

---

[5] A Bayesian approach in presenting results/sensitivities of the neutrino mass hierarchy has been proposed in Ref. [19].

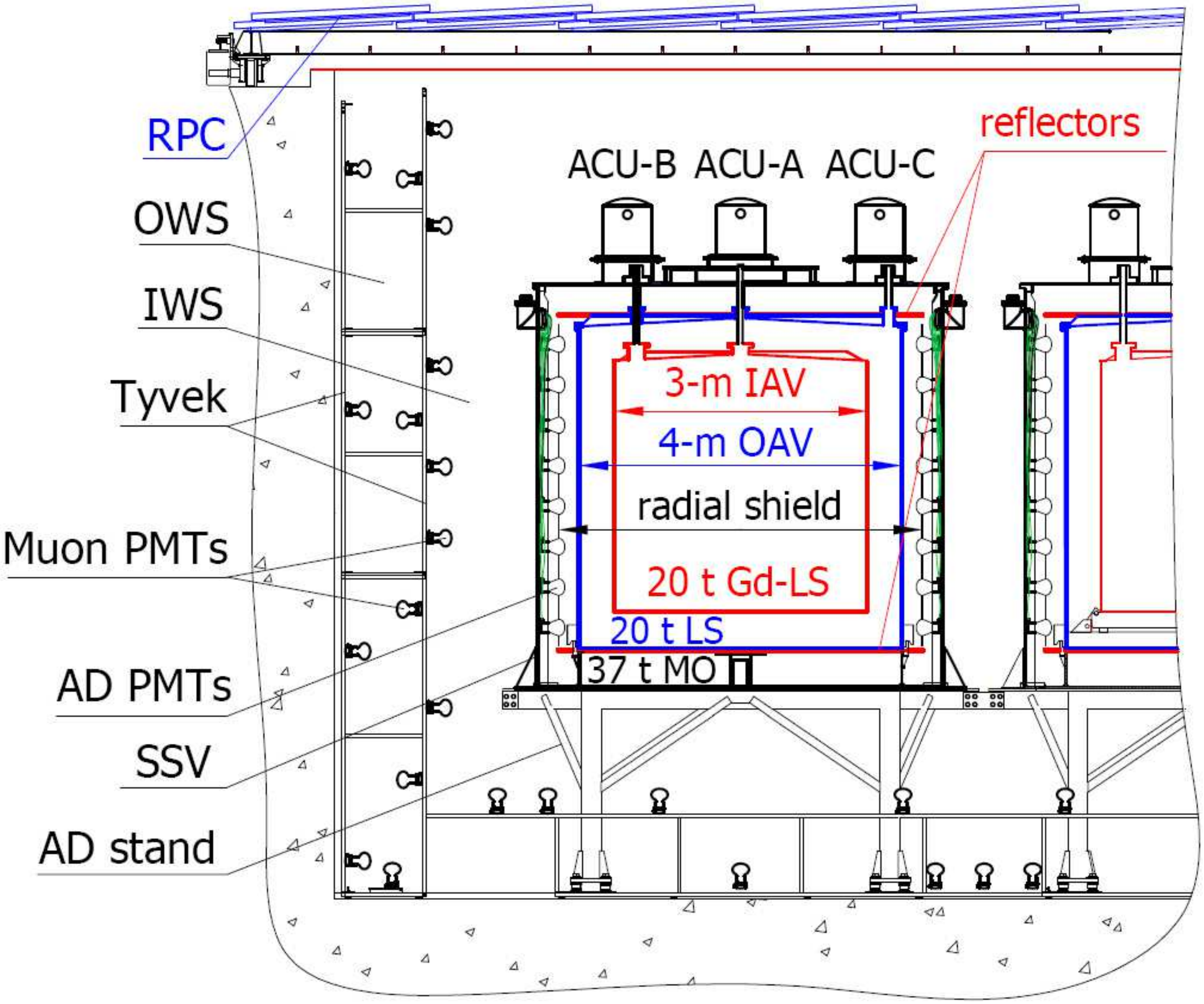
RPC
OWS
IWS
Tyvek
Muon PMTs
AD PMTs
SSV
AD stand
reflectors
ACU-B
ACU-A
ACU-C
3-m IAV
4-m OAV
radial shield
20 t Gd-LS
20 t LS
37 t MO